



THE UNIVERSITY *of* EDINBURGH

Edinburgh Research Explorer

Measurement of water vapor adsorption isotherms in mesoporous materials using the zero length column technique

Citation for published version:

Centineo, A & Brandani, S 2020, 'Measurement of water vapor adsorption isotherms in mesoporous materials using the zero length column technique', *Chemical Engineering Science*, vol. 214, 115417. <https://doi.org/10.1016/j.ces.2019.115417>

Digital Object Identifier (DOI):

[10.1016/j.ces.2019.115417](https://doi.org/10.1016/j.ces.2019.115417)

Link:

[Link to publication record in Edinburgh Research Explorer](#)

Document Version:

Peer reviewed version

Published In:

Chemical Engineering Science

General rights

Copyright for the publications made accessible via the Edinburgh Research Explorer is retained by the author(s) and / or other copyright owners and it is a condition of accessing these publications that users recognise and abide by the legal requirements associated with these rights.

Take down policy

The University of Edinburgh has made every reasonable effort to ensure that Edinburgh Research Explorer content complies with UK legislation. If you believe that the public display of this file breaches copyright please contact openaccess@ed.ac.uk providing details, and we will remove access to the work immediately and investigate your claim.



1 Measurement of water vapor adsorption isotherms in
2 mesoporous materials using the zero length column
3 technique.

4 *Alessio Centineo, Stefano Brandani**

5 School of Engineering, Institute for Materials and Processes, The University of Edinburgh, EH9
6 3FB, UK

7 **Keywords:** Water adsorption; Hysteresis loop; Scanning curves; Zero length column; Equilibrium

8 **Abstract**

9 Measurement of water adsorption isotherms is important for industrial applications and for the
10 characterization of nanoporous materials. The zero-length column technique is used for the first
11 time to measure the adsorption-desorption isotherm of water on a mesoporous adsorbent, SBA-15,
12 up to 90 % relative humidity at 298 K. The technique showed two key advantages; a) The
13 experimental flexibility for the measurement of continuous adsorption-desorption isotherms
14 characterized by complex shapes and hysteresis loops; b) The possibility to measure a complete
15 set of adsorption-desorption isotherms and scanning curves in few days compared to several weeks
16 needed with traditional gravimetric techniques. The adsorption isotherm measured was compared
17 and validated against isotherms measured on a commercial gravimetric system designed for water
18 vapor adsorption. For the system considered, the adsorption and desorption branches are very
19 steep, and the zero-length column technique is shown to allow setting easily the starting point of
20 the scanning curves.

22 **1. Introduction**

23 The commercial and industrial applications which justify the growing interest in water vapor
24 adsorption are numerous including gas drying (Ahn and Lee, 2004, 2003), food conservation (Qiu
25 et al., 2019), storage of pharmaceuticals (Waterman and Macdonald, 2010), construction materials
26 (Canivet et al., 2014), adsorption refrigeration cycles (Ruzhu Wang; Liwei Wang; Jingyi Wu,
27 2014) and, more recently, characterization of porous materials (Cychosz et al., 2017; Nguyen et
28 al., 2014; Thommes et al., 2013, 2011; Velasco et al., 2016).

29 The utilization of water adsorption for the structural characterization of porous solids is due to its
30 peculiar characteristics as adsorptive. Water vapor can specifically interact with the chemical
31 groups on the surface of the solid adsorbents. In addition, water molecules are quite small, and
32 they can easily penetrate even the tightest pores. These aspects allow water to be exploited as a
33 probe molecule for surface chemistry investigations as well as for pore structure analysis. It can,
34 therefore, be considered as a characterization method supplementary to the traditional methods
35 operated with nitrogen, argon and carbon dioxide (Thommes et al., 2015, 2011). In addition,
36 compared to the techniques based on nitrogen and argon adsorption at cryogenic conditions, water
37 adsorption experiments can be performed at room temperature. To appreciate the potential
38 advantages in using water for pore structural characterization, one might consider a typical water
39 adsorption isotherm on a microporous carbon material (Thommes et al., 2012). Either nitrogen or
40 argon, at their respective saturation temperatures, show a type I isotherm. Water, instead, shows a
41 type IV isotherm with a relevant hysteresis loop due to the different adsorption-desorption
42 mechanisms and to the capillary condensation phenomena (Sarkisov et al., 2017; Thommes et al.,

43 2012). The option to have two distinct branches potentially offers elements for a more accurate
44 characterization of the pore structure. However, a more complex understanding and modeling of
45 the phase behavior of water on a molecular scale is needed for an accurate evaluation, not only of
46 the surface chemistry but also of the pores dimension and structure (Sarkisov et al., 2017).

47 Water vapor adsorption isotherms have traditionally been measured using either gravimetric or
48 volumetric techniques (Baker and Sing, 1976; Naono et al., 1980; Rajniak and Yang, 1993;
49 Sarkisov et al., 2017; Velasco et al., 2016). The easiest and cheapest method consists in measuring
50 the mass change of a solid adsorbent when exposed to a gas phase in equilibrium with an over-
51 saturated salt solution (Young, 2007). However, such a method is extremely time consuming and
52 the accuracy of the experimental data can be quite poor. Commercial gravimetric instruments are
53 typically dynamic sorption systems in which a humid stream and a dry stream are continuously
54 mixed and sent inside the weighing chamber of the instrument. Such instruments are very accurate
55 in a wide range of relative humidity but rather expensive. However, they suffer a lack of accuracy
56 of the humidity detectors at very low concentrations and, therefore, it is generally not possible to
57 evaluate correctly the Henry's law constant. Commercial volumetric instruments are very accurate
58 and comparable in price to the gravimetric ones. These instruments are reasonably faster than the
59 gravimetric ones, as the experiments are performed without the use of a carrier gas. Moreover,
60 they also allow the accurate measurement of the equilibrium isotherm in the entire concentration
61 range, Henry's law constant included, provided that water adsorption on the surfaces of the
62 instruments is minimized. All the techniques mentioned so far can typically be considered as the
63 most common ways to measure adsorption-desorption equilibrium isotherms on solid adsorbents.

64 These techniques operate in a discontinuous mode, measuring a single point on the isotherm at
65 each step. The partial pressure of the adsorptive is adjusted according to a stepwise ramp and the

66 uptake of adsorbate into the solid is measured for each step. This way of operating is time-
67 consuming if accurate measurements are to be performed. Moreover, the equilibration time and/or
68 the amount of gas dosed for each single concentration step cannot be accurately decided *a priori*
69 and some trial runs are needed to optimize the experimental parameters. Each trial run on a
70 gravimetric or volumetric technique can take several days. This aspect is particularly relevant for
71 solids characterized by almost vertical adsorption or desorption branches. For these solids, the
72 capillary condensation/evaporation branches extend over an extremely small pressure range. The
73 measurement of the scanning curves is, therefore, not trivial as the starting points lie on a highly
74 tight region of the isotherm. In this particular case, extremely stable concentrations of the gas phase
75 are needed in the gravimetric technique, meanwhile, accurate values of dosed volumes are required
76 in the volumetric techniques.

77 Chromatographic techniques, such as the Zero Length Column (ZLC), can be tailored and used for
78 more rapid measurements of continuous adsorption-desorption isotherms (Brandani and Ruthven,
79 2003; Brandani et al., 2003). The ZLC was initially introduced and developed as a fast and reliable
80 chromatographic method for diffusion measurements of adsorptives in microporous solids
81 (Brandani and Ruthven, 1996a; Eic and Ruthven, 1988). The main assumptions made for the
82 formulation of the original model are perfectly-mixed gas phase, linear equilibrium isotherm,
83 monodispersed and microcrystalline solid adsorbent, intracrystalline or microporous diffusion
84 mechanism, constant outlet flowrate equal to the carrier flowrate, negligible thermal effects, and
85 negligible pressure drops. In the following years, the original model has been extended to consider
86 the non-linearity of the adsorption isotherm (Brandani, 1998; Brandani et al., 2000), biporous
87 adsorbents (Brandani, 1996), solids with particle or crystal size distributions (Duncan and Moller,
88 2002), and variable outlet flowrate (Brandani, 2005; Wang et al., 2011). Until now the technique

89 has been extensively and almost exclusively adopted for kinetic measurements. However, a ZLC
90 can work both under kinetic control conditions and under dynamic-equilibrium control conditions.
91 Therefore, the technique permits one to measure either mass transfer coefficients or adsorption-
92 desorption isotherms. The variable which is experimentally used to achieve the transition from
93 dynamic-equilibrium control to kinetic control is the carrier gas flowrate. A simple graphical check
94 can assess whether the system is under equilibrium or kinetic control conditions (Brandani, 2016;
95 Mangano et al., 2013).

96 The ZLC technique has previously been modeled and tested for the measurement of the adsorption
97 isotherms for single and multicomponent systems (Brandani et al., 2003; Brandani and Ruthven,
98 2003). Several adsorptives on different microporous solids were tested. Both linear and type I
99 adsorption isotherms were measured. The adsorption isotherm can be computed from the
100 experimental concentration curves in two different ways. The easiest way for single adsorbates
101 consists in integrating the overall mass balance in the column using the experimental concentration
102 signal at the outlet of the column (Brandani et al., 2003). The average amount adsorbed is directly
103 obtained as a function of the gas phase concentration. This method is the most recommended since
104 it provides the adsorption isotherm from a simple and robust integration of the experimental
105 concentration signal at the outlet of the column. It is also useful when the shape of the isotherm is
106 not known *a priori*. The alternative method is based on the simulation and best-correlation of the
107 ZLC response curves (Friedrich et al., 2015). In such a case, a model for the adsorption equilibrium
108 isotherm and a model for the mass transfer kinetics are needed. The system of differential equations
109 given by the overall mass balance in the system and the mass balance in the solid is to be solved
110 to correlate the gas phase concentration-response curves. Under equilibrium control conditions,
111 the shape of the simulated response curves will only depend on the adsorption isotherm parameters.

112 Therefore, the isotherm parameters can be computed from the best-correlation of the experimental
113 curves.

114 The use of the ZLC technique for the measurement of adsorption isotherms has been demonstrated
115 only for type I isotherms and has been validated and shown to be in good agreement with data
116 from gravimetric or volumetric systems (Brandani et al., 2003). In addition, the experiments
117 conducted with the ZLC system are much faster given that a complete equilibrium isotherm could
118 be measured in few minutes (Brandani et al., 2003). The ZLC technique is, therefore, a potentially
119 useful approach for the very time-consuming measurement of water adsorption isotherms in
120 mesoporous materials.

121 In this contribution, the use of the ZLC technique has been extended to the measurement of
122 continuous adsorption-desorption type-IV isotherms for water vapor on SBA-15. The theoretical
123 basis with the underlying assumptions that allow to use the ZLC system is discussed in order to
124 establish the experimental checks that must be performed. The experimental procedure will be
125 presented with particular attention to the modifications of a traditional ZLC system for adsorption
126 measurements of highly concentrated vapors and the experimental results are validated with
127 independent measurements on a gravimetric system that include desorption and adsorption
128 scanning curves.

129 **2. ZLC equilibrium theory**

130 The main assumption used in modelling the ZLC (Zero Length Column) technique is to consider
131 the length of the packed bed small enough to allow a negligible gradient of the gas phase
132 concentration along the column (Aris, 1991; Eic and Ruthven, 1988). In such a scenario, the
133 column can be considered as a perfectly mixed tank and the concentration is assumed to be the

134 same in each point of the gas phase inside the bed. The thermal effects and the pressure drop in
 135 the column are practically negligible. Under these assumptions, the overall mass balance on the
 136 adsorptive and on the adsorbed phase inside the column reduces to a quite simple form that can be
 137 expressed as (Brandani et al., 2003; Brandani and Ruthven, 1996a):

$$138 \quad V_s \frac{d\bar{q}}{dt} + V_f \frac{dc}{dt} = F_{in}c_{in} - F_{out}c \quad (1)$$

139 Where \bar{q} is the average concentration in the solid; c is the vapor phase concentration inside the
 140 column; c_{in} is the vapor phase concentrations at the inlet of the column; V_s is the solid adsorbent
 141 volume in the column; V_f is the gas phase volume in the column; F_{in} and F_{out} are respectively the
 142 volumetric flowrate at the inlet and at the outlet of the column; and t is time.

143 The ZLC can work either under equilibrium or kinetic control conditions. The ZLC is a dynamic
 144 measurement technique in which the gas and the adsorbed phase concentrations are continuously
 145 changing during the experiment. In this scenario, the dynamic equilibrium measurements are to be
 146 interpreted as a series of infinitesimal equilibrium steps. To ensure that the adsorbed phase average
 147 concentration is at equilibrium with the gas phase concentration at any time, at least two
 148 experiments at different flowrate must be performed (Brandani, 2016). If the experimental curves
 149 measured at different flowrates overlap on a c vs $F_{out}t$ plot (Ft -plot), the amount adsorbed will
 150 only depend on the amount of gas passed through the column, and the system can be considered
 151 under equilibrium control conditions.

152 Eq. (1) can be integrated with respect to time:

$$153 \quad V_s[\bar{q}(t) - \bar{q}(0)] + V_f[c(t) - c(0)] = \int_0^t F_{in}c_{in}dt - \int_0^t F_{out}c(t)dt \quad (2)$$

154 In an adsorption experiment: $\bar{q}(0) = 0$; $c(0) = 0$; and $c_{in} = c_0$ is set, while $c(t)$ is measured. F_{in}
 155 is also assigned while F_{out} can either be measured or can be approximated to high accuracy from

156 the measured concentration of the adsorptive (Brandani et al., 2003; Malek and Farooq, 1996). V_f
 157 , the volume of the gas phase inside the column, is determined from blank experiments (Brandani
 158 et al., 2003).

159 In a desorption experiment: $\bar{q}(0) = q_0$; $c(0) = c_0$; and $c_{in} = 0$ is set, while $c(t)$ is measured. If
 160 the adsorption experiment is carried out to full equilibration, then (c_0, q_0) is the first point on the
 161 adsorption isotherm.

162 For a blank experiment, Eq. (2) simplifies to:

$$163 \quad V_f[c(t) - c(0)] = \int_0^t F_{in}c_{in}dt - \int_0^t F_{out}c(t)dt \quad (3)$$

164 Which allows to determine the final unknown, V_f .

165 While more complicated expressions for the variation of flowrate with time are available (Wang
 166 et al., 2011), in the case of water isotherms, the mole fraction of the adsorptive is typically below
 167 0.05 and without loss of accuracy it is possible to calculate the outlet flowrate from the measured
 168 concentration and the carrier gas flowrate (Brandani et al., 2003; Malek and Farooq, 1996):

$$169 \quad F_{out}(t) = \frac{F_{in}(1-y_{in})}{1-y(t)} = \frac{F_{carr}}{1-\frac{c(t)}{c_T}} \quad (4)$$

170 Where $c_T = \frac{P}{RT}$ is the molar concentration of the gas phase having assumed ideal gas behaviour;
 171 y_{in} is the molar fraction of water vapour at the inlet of the column and $y(t)$ is the molar fraction
 172 of water vapour in the column. In applying Eq. (2) to the desorption experiments it is useful to
 173 consider that the long-time asymptotic response of a ZLC system will be a single exponential
 174 decay. In this region the flowrate will also reduce to that of the carrier gas and therefore the
 175 integration can be split into two regions. A numerical integral up to a time t_{Exp} , followed by the

176 analytical integral of the exponential decay $a \exp(-bt)$ (Brandani and Ruthven, 1996b), which
 177 corresponds to the Henry law region (Brandani et al., 2003):

$$178 \int_{t_{Exp}}^{\infty} F_{carr} a \exp(-bt) dt = F_{carr} \frac{a}{b} \exp(-bt_{Exp}) \quad (5)$$

179 Provided that the experiment is carried out under equilibrium control conditions, it is therefore
 180 straightforward to obtain the experimental adsorption isotherm from an integral of the measured
 181 signal.

182 **2.1.ZLC response curves for different isotherms**

183 Given that all previous measurements of adsorption isotherms have been carried out for type I
 184 isotherms, it is important to understand what differences are to be expected in the dynamic
 185 response of a ZLC system when different isotherms are considered.

186 Under equilibrium control conditions, $\bar{q}(t) = q_{eq}[c(t)]$ and the mass balance in the system, Eq.
 187 (1), can be expressed as:

$$188 \left(V_s \frac{dq_{eq}}{dc} + V_f \right) \frac{dc}{dt} = F_{in} c_{in} - F_{out} c \quad (6)$$

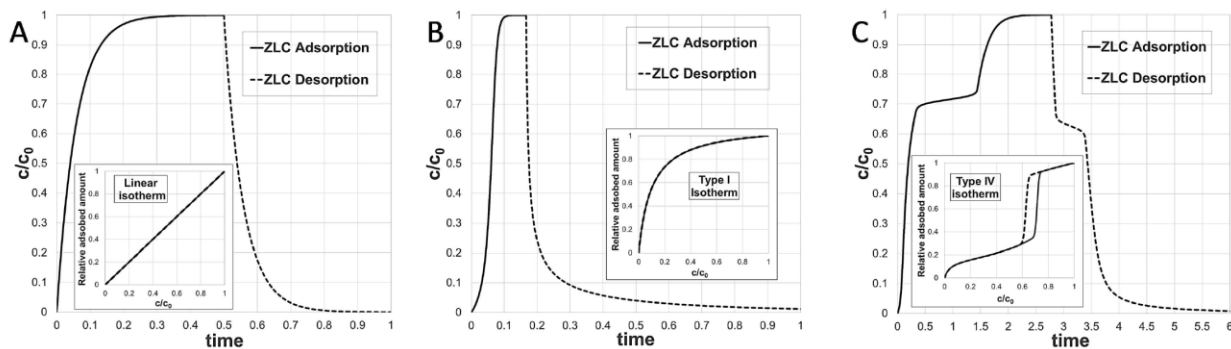
189 Where dq_{eq}/dc is the derivative of the equilibrium isotherm. By assuming different isotherms
 190 linear, Langmuir and type IV, Eq. (5) can be integrated to obtain $c(t)$ and the results can be
 191 normalised defining

$$192 C = c/c_0 \quad (7)$$

$$193 Q = q_{eq}/q_0 \quad (8)$$

$$194 \gamma = V_f c_0 / V_s q_0 \quad (9)$$

195 The simulated ZLC response curves for $\gamma = 0.05$ are reported in Fig. 1 for the different isotherms.



196

197 **Fig. 1.** (A) Adsorption-Desorption equilibrium isotherm and ZLC response curves simulated under
 198 equilibrium control conditions. Linear isotherm. (B) Adsorption-Desorption equilibrium isotherm
 199 and ZLC response curves simulated under equilibrium control conditions. Type I isotherm. (C)
 200 Adsorption-Desorption equilibrium isotherm and ZLC response curves simulated under
 201 equilibrium control conditions. Type IV isotherm.

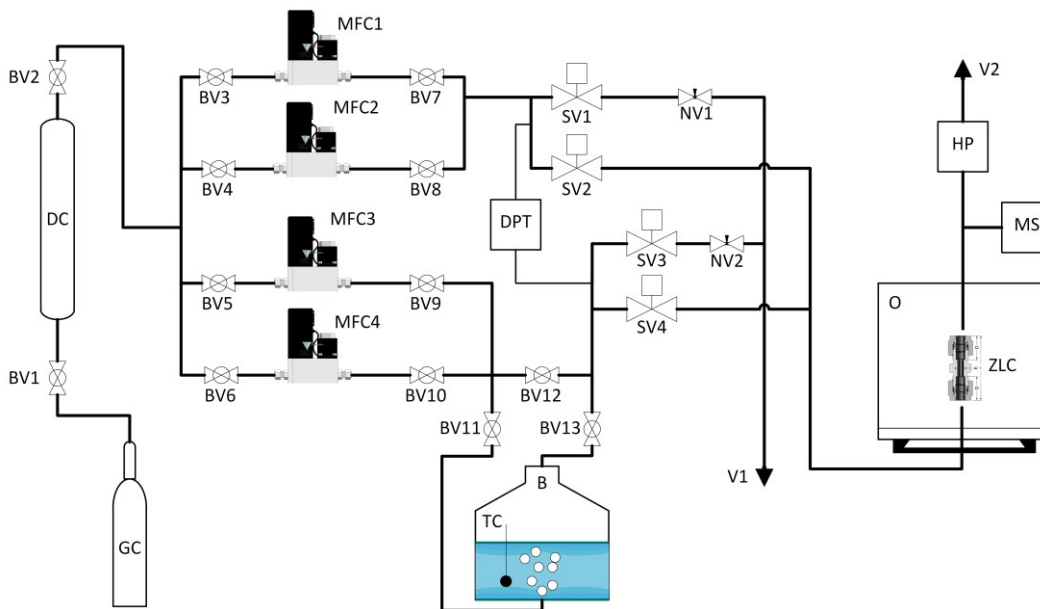
202 Fig. 1a shows the characteristic symmetry of linear systems. Fig. 1b shows the typical asymmetric
 203 response of nonlinear type I systems, with the long tail in the desorption curve associated with the
 204 Henry law region. Fig. 1c shows a very interesting shape, with the condensation and evaporation
 205 branches corresponding to plateaus in the vapor phase concentration signal. It is interesting to note
 206 that what is a nearly vertical branch in a normal experiment, becomes a protracted (in time)
 207 horizontal branch in the ZLC response curve.

208 3. Materials and Methods

209 3.1. ZLC apparatus

210 The experimental apparatus used in this work is a purposely designed ZLC system. The simplified
 211 flowsheet of the apparatus is presented in Fig. 2. Dry nitrogen was used as carrier gas. The dry
 212 nitrogen flowrate is controlled by two 0-5 ml/min and two 0-250 ml/min SLA5850S BROOK mass

213 flow controllers. The accuracy of these mass flow controllers is $\pm 1.0\%$ of rate (20% - 100% FS)
214 and $\pm 0.2\%$ FS (below 20% FS). A 100 ml bubbler was used for the humidification of the feed line.
215 The bubbler is provided with a sparger and a demister for trapping droplets carried over by the gas
216 flow. The bubbler was immersed in a HAAKE K20 temperature-controlled bath with a DC30
217 circulator. The temperature of the bath was used to set the relative humidity of the wet nitrogen at
218 the inlet of the column. To avoid water vapor condensation, all the lines containing humid nitrogen
219 were carefully kept hot by using Omega Engineering heating ropes powered by Electrothermal
220 MC5 heating controllers. The lines were insulated with fiberglass tape. Two detectors were used
221 for the analysis of the concentration curves at the outlet of the ZLC: the first one is a quadrupole
222 Ametek Dycor Dymaxion mass spectrometer which continuously samples a flowrate of about 0.02
223 ± 0.01 ml/min of gas at the outlet of the ZLC through a silica fused capillary. The second detector
224 is a Rotronic HC2-SM humidity and temperature probe connected after the MS capillary and in
225 series with the ZLC. This probe has an accuracy of $\pm 0.8\%$ rh / ± 0.1 K and is the same model as
226 the humidity probe in the Aquadyne instrument. The signal of the MS was used to integrate the
227 mass balance given in Eq. (1). The signal of the humidity probe was used to measure the absolute
228 concentration of water vapor at the inlet of the column, c_0 . This value is relevant for the correct
229 evaluation of the mass balance and for the position of the calculated isotherm with respect to the
230 x-axis. The relative humidity value measured by the humidity probe was approximately 95 % of
231 the equilibrium humidity value expected from the bubbler. The adsorption column was inserted
232 inside a Carbolite 3216 oven which can reach a max temperature of 350 °C.



233

234 **Fig. 2.** Schematic flowsheet and components of the experimental ZLC system. GC carrier gas
 235 cylinder; DC drying column; BV ball valve; NV needle valve; TC water bath temperature
 236 controller; MFC mass flow controllers; B water bath; SV solenoid switching valve; V vent; O ZLC
 237 oven; ZLC zero length column; DPT differential pressure transducer; HP humidity probe; MS
 238 mass spectrometer.

239 The differential pressure between the adsorption and desorption lines was measured by means of
 240 a GE Unik 5000 differential pressure transducer. Two Swagelok metering valves were used at the
 241 vents to equilibrate the pressures in the two lines before switching the valves. The switch between
 242 the adsorption and desorption line was operated using four Shako solenoid valves. A commercial
 243 Quantachrome Aquadyne DVS gravimetric system was used to validate the experimental
 244 isotherms obtained with the ZLC. This gravimetric apparatus uses also a Rotronic humidity probe
 245 with the same accuracy as that on the ZLC system.

246 **3.2. Sample preparation and loading**

247 The details of the synthesis and preparation of the adsorbent material used in this contribution can
248 be found in the literature (Chiang et al., 2016). A SEM image of the solid is shown in Fig. 3. The
249 mass of solid was measured with a Mettler Toledo XS205 balance (guaranteed repeatability of
250 ± 0.05 mg) inserted inside a glove box with a continuous nitrogen flow to minimize the amount of
251 moisture in the gas phase. Two columns were packed respectively with 3.7 mg and 1.2 mg of solid
252 adsorbent. Prior to the first experimental run, the solid was activated *in situ* at 393 K for 3 hours
253 under nitrogen flow. The ZLC experiments were conducted by performing several reversible
254 adsorption-desorption cycles on the same batch. As discussed in a previous study (Centineo et al.,
255 2019). during the first adsorption step the material changes irreversibly, trapping part of the water.
256 Following the first experiment all the isotherms become reversible and in this study we consider
257 only these conditions and compare the results to the gravimetric experiments from repeated
258 exposure to water (Centineo et al., 2019).



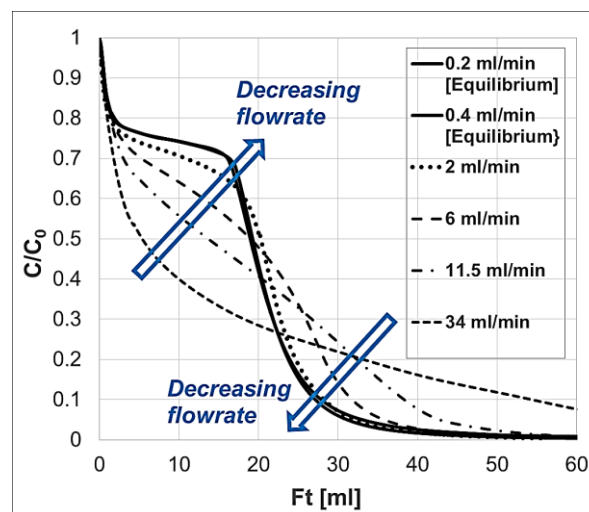
259
260 **Fig. 3.** SEM image of SBA-15 sample used in this study.

261 4. Results and Discussion

262 4.1. Main adsorption-desorption curves

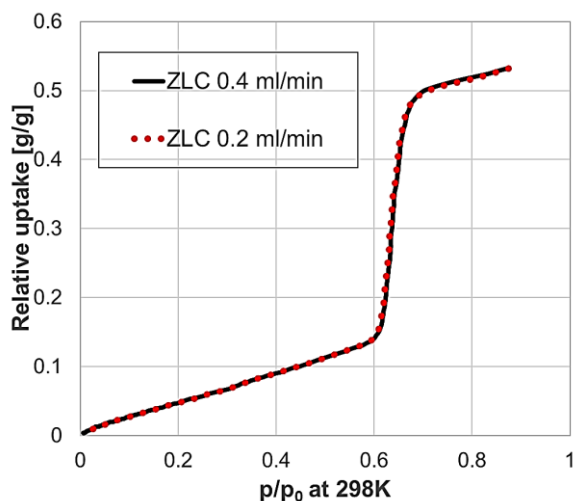
263 The initial experiments were aimed to assess the control regime of the system for different
264 desorption flowrates. Several experiments, at the same temperature and same initial concentration,
265 were performed to find out the highest flowrate at which the system could be considered under
266 equilibrium control conditions. As discussed beforehand, a plot of the experimental C vs Ft
267 represents a simple and reliable graphical check for the assessment of the control regime of the
268 system (Brandani, 2016).

269 The different control regimes can clearly be observed in Fig. 4 where several desorption curves
270 measured at different flowrates are plotted on an Ft -plot. At the highest flowrate, the shape of the
271 response curve is similar to that of a type-I isotherm. It is therefore essential to be able to change
272 the flowrate until overlap of curves on the Ft -plot is achieved.



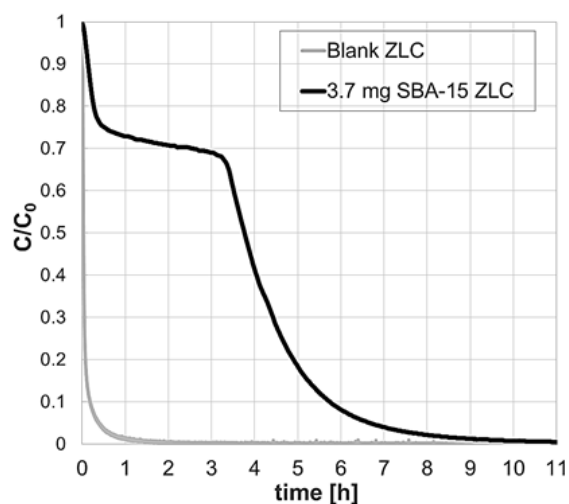
273
274 **Fig. 4.** Experimental Ft -plot for the evaluation of the control regime. Sample mass 1.2 mg. Initial
275 relative humidity = 86 %, at 298K and atmospheric pressure.

276 When the flowrate is sufficiently low, the response curves approach the equilibrium regime and
277 the effect of the shape of the isotherm becomes clearly visible. Indeed, the curves obtained at the
278 two lowest flowrates overlap completely and, therefore, these can be considered under equilibrium
279 control conditions and the integral can be performed to obtain the measured desorption isotherm
280 shown in Fig. 5. It must be considered that the mass spectrometer can acquire data at high
281 frequency and, therefore, practically continuous adsorption-desorption isotherms can be obtained.
282 Fig. 5 is, in fact, a curve with 10^4 experimental points and the integration procedure helps also in
283 smoothing the noise of the original signal. As this is the first time that such an isotherm is obtained
284 from a ZLC measurement, it is worth noting that extremely low flowrates, less than 1 ml/min, are
285 required to reach equilibrium control conditions. This implies also the need to couple the ZLC
286 system to a mass spectrometer that has a very low inlet flowrate in the capillary. Not all commercial
287 quadrupole mass spectrometers can be used in this configuration unless a make-up gas is used, but
288 this then dilutes the signal.

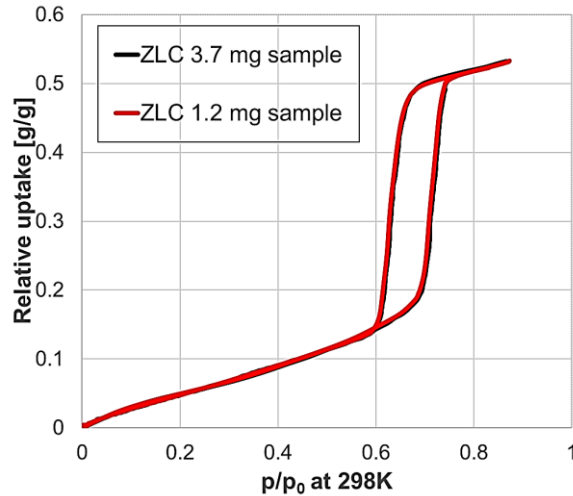


289
290 **Fig. 5.** Desorption isotherm calculated by using the two lowest flowrates shown in Fig. 4. Sample
291 mass 1.2 mg. Initial relative humidity = 86 % at 298K and atmospheric pressure.

292 The fact that at higher flowrates the system is under kinetic control indicates that it is also possible
293 to use the same instrument to measure kinetic properties, but the focus of this contribution is that
294 of determining accurate equilibrium properties. It is important to note that the interpretation of
295 kinetic experiments requires the knowledge of the derivative of the adsorption isotherm (Chmelik
296 and Kärger, 2016; Glover et al., 2008; Hefti et al., 2015; Kärger et al., 2012; Lin et al., 1996;
297 Ruthven, 1984) and clearly this can be estimated accurately from ZLC measurements given the
298 large number of points available, particularly in the adsorption and desorption branches.
299 The blank response of the system, which is used to calculate V_f in Eq. (1), is practically negligible
300 if compared to the desorption run (Fig. 6). Moreover, to verify the assumption of negligible thermal
301 effects and pressure drops, the adsorption-desorption isotherm was measured with two different
302 masses of sample showing a near-perfect reproducibility (Fig. 7).



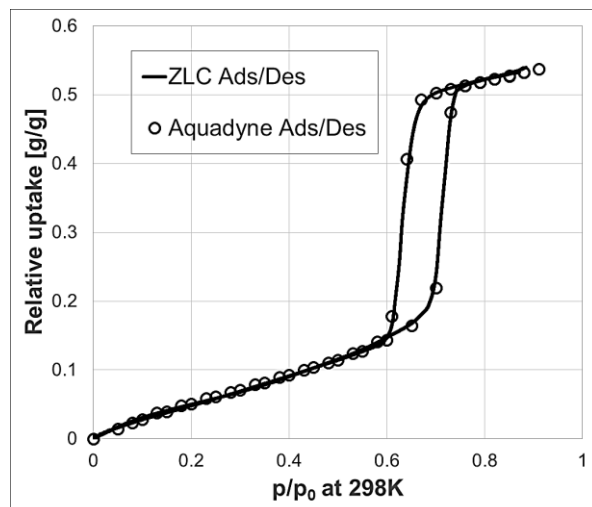
303
304 **Fig. 6.** Experimental response curves for the blank column and packed column. Sample mass 3.7
305 mg. Initial relative humidity = 86 % at 298K and atmospheric pressure.



306

307 **Fig. 7.** Adsorption and desorption isotherms measured using two different sample masses. Initial
 308 relative humidity = 86 % and atmospheric pressure.

309 Fig. 8 shows the continuous isotherm calculated from the ZLC signal and the equilibrium isotherm
 310 measured on the gravimetric system used as reference. The excellent agreement between the two
 311 isotherms measured with two independent systems validates the experimental protocols used in
 312 the ZLC technique and confirms that the possible uncertainty is within 2% which corresponds
 313 approximately to the size of the symbols used for the gravimetric data. The main advantage of the
 314 ZLC measurement is particularly evident in the adsorption and desorption branches. It is very
 315 difficult to measure several points in these regions using the gravimetric system and as a result,
 316 there is a much larger uncertainty in the slope of the isotherm in these regions. Given that this is
 317 where the kinetic limitations are more evident (see Fig. 4), it is also the region where an accurate
 318 estimate of the derivative of the isotherm is needed for the interpretation of kinetic experiments.

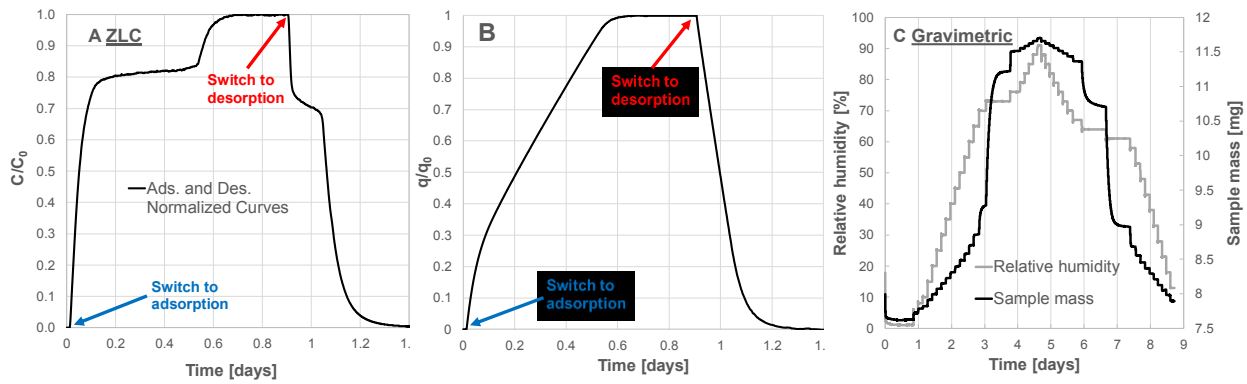


319

320 **Fig. 8.** Comparison between the isotherms measured with the ZLC system and gravimetric system.
 321 ZLC sample mass 3.7 mg. Gravimetric sample mass 7 mg. Initial relative humidity = 86 % and
 322 atmospheric pressure. Experimental signals are shown in Fig. 9.

323 Fig. 9 shows the second remarkable advantage of the ZLC technique. Given that the entire isotherm
 324 is determined continuously, the time needed to produce the full adsorption and desorption cycle is
 325 approximately 1.4 days compared to 9 days of the gravimetric experiment. In the gravimetric
 326 experiment, one could reduce the time needed by reducing the number of points on the curves,
 327 since the limiting process is the equilibration time of the individual points but to have a sufficiently
 328 detailed isotherm one would still need several days to one week. Here clearly one can see the
 329 potential of coupling a ZLC system with a gravimetric or volumetric apparatus since the ZLC can
 330 provide an accurate shape of the isotherm rapidly, while the single point-based measurements can
 331 provide an independent confirmation of the absolute accuracy of the ZLC results. This can be
 332 important when very small sample masses are used in the ZLC measurement.

333



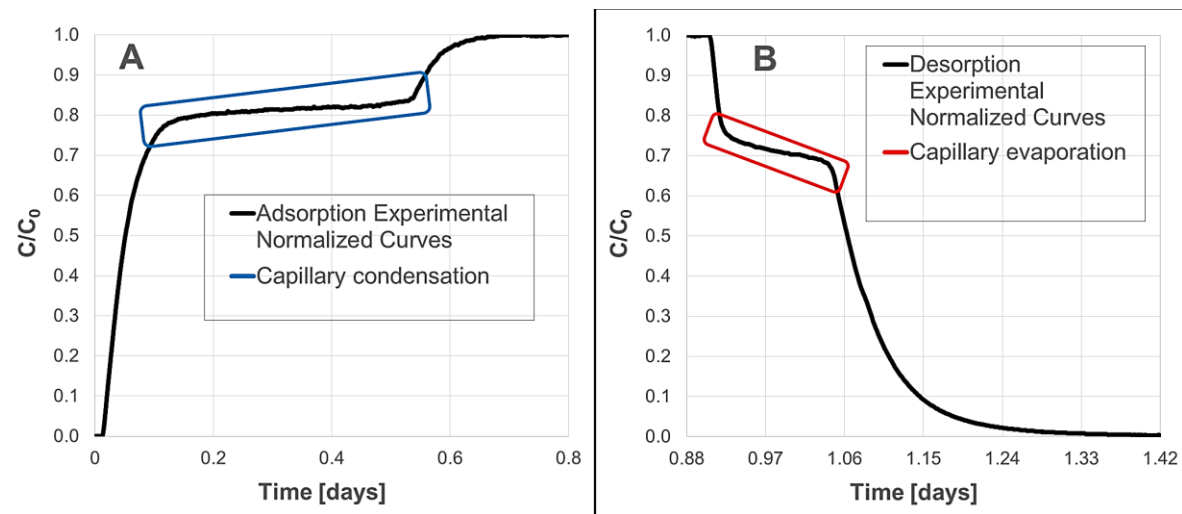
334

335 **Fig. 9.** (A) Experimental adsorption-desorption normalized response curves measured under
336 equilibrium control conditions on the ZLC. (B) Adsorbed phase concentration vs time obtained
337 from ZLC mass balance. Sample mass 3.7 mg. Highest relative humidity = 86 % at 298K and
338 atmospheric pressure. (C) Experimental uptake curves obtained from the measurement of the
339 equilibrium adsorption-desorption isotherm on the gravimetric system. Sample mass 7 mg.

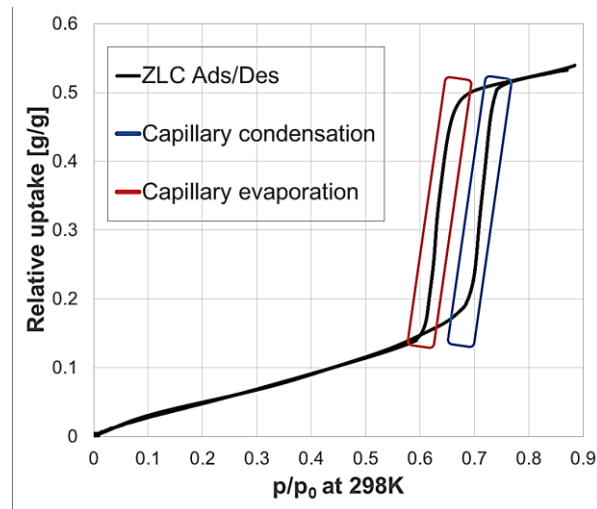
340 4.2.Scanning curves

341 The advantages of the ZLC extend to the measurement of the scanning curves, i.e. the curves which
342 scan the hysteresis loop from the adsorption branch to the desorption branch and *vice versa*. These
343 curves are defined as adsorption or desorption scanning curves according to the starting point and
344 direction along the equilibrium isotherm (Monson, 2012). The trajectory of these curves is strictly
345 correlated to the pore structure of the solids (Cychosz et al., 2017). Scanning curves have recently
346 gained interest as a powerful and essential tool for the systematic characterization of the inner
347 structure of nanoporous solids (Cordero et al., 2002; Cychosz et al., 2017; Klomkliang et al., 2015,
348 2014; Monson, 2012; Morishige, 2017; Sarkisov et al., 2017; Tompsett et al., 2005; Zeng et al.,
349 2016). Therefore, the possibility to measure continuous and accurate scanning curves would
350 represent a considerable step forward in the structural characterization of porous solids.

351 For the efficient measurement of the scanning curves, it is important to appreciate the correlation
352 between the shape of the signal and the isotherm. In the ZLC experiment the measured quantity is
353 the partial pressure of water, therefore the adsorption and desorption branches result in horizontal
354 plateaus where the isotherm is very sharp. This is clearly highlighted in Fig. 10, which shows the
355 normalized signal vs time. Fig. 11 shows the regions corresponding to the two plateaus in the
356 isotherm.



357
358 **Fig. 10.** Experimental normalized response curves measured under equilibrium control conditions
359 on the ZLC at 298K and atmospheric pressure. Sample mass 3.7 mg. (A) Measurement of the main
360 adsorption branch. Final relative humidity = 86 %. (B) Measurement of the main desorption
361 branch. Initial relative humidity = 86 %.



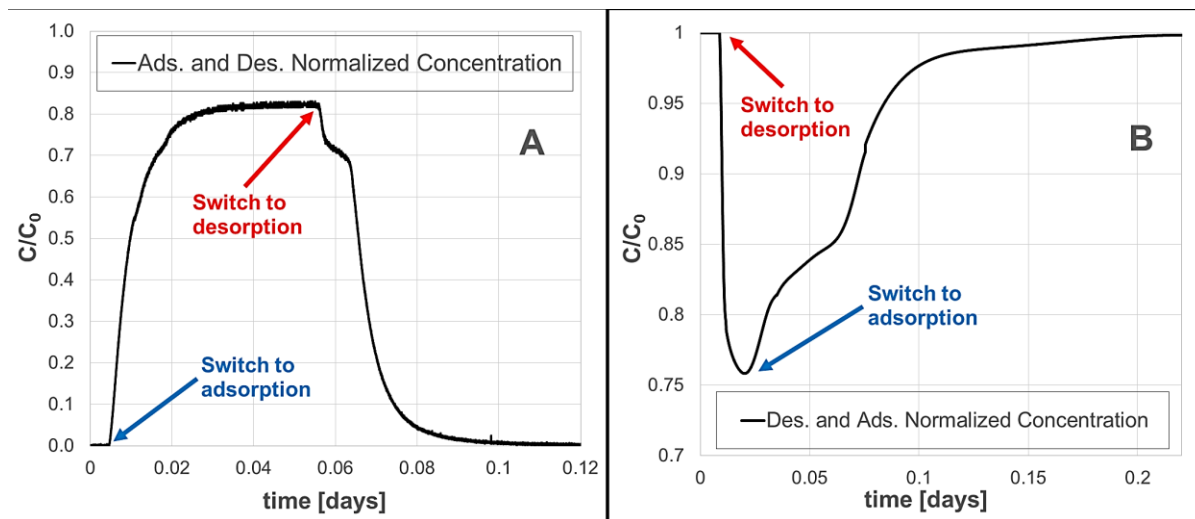
362

363 **Fig. 11.** Experimental adsorption-desorption isotherm calculated from the ZLC response curves
 364 shown in Fig. 10. Sample mass 3.7 mg. Highest relative humidity = 86 % at 298K and atmospheric
 365 pressure.

366 From Fig. 10, if the valve is switched at any time between 0.15 and 0.55 days a desorption scanning
 367 curve is obtained. Figure 9B can be used to determine the adsorbed phase concentration at the start
 368 of the scanning experiment. This should be compared to setting the partial pressure in a traditional
 369 experiment to between 70 and 73% relative humidity. Even with a very accurate control of the
 370 relative humidity, performing more than 2 scanning curves at precise locations is a challenge using
 371 a single-point based technique. On the other hand, with the ZLC one can automate the valve
 372 switching times and could generate a large number of scanning curves without difficulty. A similar
 373 analysis applies to the desorption branch, which extends between 0.9 and 1 day, i.e. more than 2
 374 hours. This is a sufficiently broad period of time to allow for several adsorption scanning curves,
 375 considering that the valve switching time is a fraction of a second.

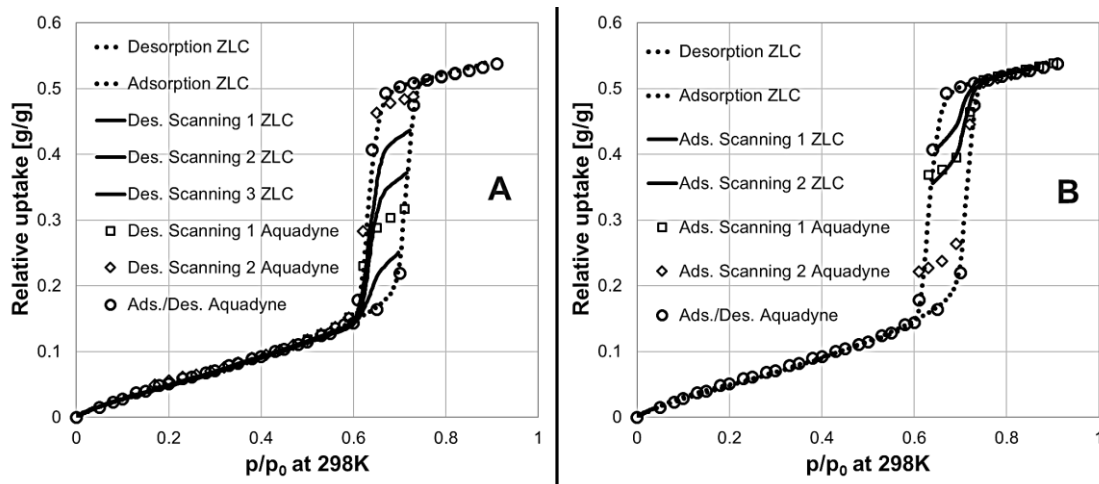
376 Just for clarity, it is important to stress that this method is based on having established the
 377 conditions for equilibrium control. Under these conditions, the adsorption or desorption
 378 experiment is run for a fixed period of time and the valve is switched while the concentrations are

379 within the hysteresis loop, to obtain scanning curves. Fig. 12 shows the experimental signal for
380 desorption and adsorption scanning curves as an example of the methodology.



381
382 **Fig. 12.** Experimental adsorption-desorption normalized response curve measured under
383 equilibrium control conditions at 298K and atmospheric pressure for sample mass 3.7 mg. (A)
384 Measurement of the desorption scanning curve, $t_{\text{switch}} = 12110$ s. Initial relative humidity = 71.5
385 %. (B) Measurement of the adsorption scanning curve, $t_{\text{switch}} = 1710$ s. Initial relative humidity =
386 64 %.

387 Fig. 13 shows the full comparison of the measured scanning curves with the ZLC and the
388 gravimetric system (under similar starting conditions). The comparisons show that again the ZLC
389 results are validated and it is clear that the continuous scanning curves have significant detail,
390 particularly in the way in which the curves join with the opposite branch. In addition, a traditional
391 gravimetric instrument would approximately require between one to two months for the accurate
392 measurement of a complete set (at least 3 different temperatures) of main adsorption/desorption
393 curves and scanning curves. The ZLC can be used to measure the same curves with more definition
394 in a single week.



395
 396 **Fig. 13.** (A) Desorption scanning curves measured on the ZLC system and gravimetric system.
 397 Initial relative humidity = 72.2 %, 71.5 % and, 69.7 %. ZLC sample mass 3.7 mg. Gravimetric
 398 sample mass 7 mg. (B) Adsorption scanning curves measured on the ZLC system and gravimetric
 399 system. Initial relative humidity = 64 % and, 64.8 %. ZLC sample mass 3.7 mg at 298K and
 400 atmospheric pressure. Gravimetric sample mass 7 mg.

401

402 5. Conclusions

403 In this contribution, the innovative and effective use of the ZLC technique for the measurement of
 404 type IV adsorption isotherms was demonstrated. The technique was able to accurately reproduce
 405 the complex shape of water vapor adsorption-desorption isotherms on SBA-15. The adsorption-
 406 desorption isotherms were obtained by means of a simple and robust integration of the ZLC
 407 response curves.

408 Experiments at different flowrates and with different sample masses were performed to exclude
 409 the presence of any thermal effects and pressure drops, thus, confirming the assumptions of the
 410 ZLC technique. Extremely low flowrates were required to approach the equilibrium control

411 conditions, suggesting a slow mass transport for water vapor into the solid. The blank experiment
412 permitted to exclude any condensation of water vapor in the lines as the response integral was
413 virtually negligible when compared to the column response.

414 The ZLC technique was coupled with a high-frequency sampling mass spectrometer which
415 permitted the calculation of what is essentially a continuous isotherm. This accurate determination
416 of the shape of the isotherm allows to calculate also the derivative of the isotherm, which is relevant
417 for kinetic studies.

418 The ZLC data were validated against the equilibrium isotherm measured on an independent
419 commercial gravimetric system designed for water adsorption measurements, showing excellent
420 agreement. One of the main advantages of the ZLC is that it is intrinsically faster, by up to an order
421 of magnitude, and can provide virtually continuous adsorption-desorption isotherms. For
422 isotherms characterized by almost vertical adsorption/desorption branches, as in the case of SBA-
423 15, the ZLC provides considerably more detail compared to any single-point equilibration
424 technique. Compared to traditional techniques the main disadvantage is that the isotherm is
425 obtained from the numerical integration of the concentration signal rather than being the directly
426 measured quantity.

427 The ZLC was also used to determine adsorption and desorption scanning curves. Another
428 significant advantage of the ZLC is the fact that the very narrow pressure ranges over which
429 condensation and evaporation occur become relatively long time intervals thus allowing to select
430 easily the starting points for scanning experiments. Obtaining virtually continuous scanning curves
431 provides increased detail, especially where the scanning curve re-joins the opposite branch of the
432 hysteresis loop.

433

434

435

436 **Corresponding Author**

437 * E-mail: s.brandani@ed.ac.uk.

438 **ORCID**

439 Stefano Brandani: 0000-0001-9470-6837

440 **Funding Sources**

441 One of the authors (A.C.) acknowledges the support received from The University of Edinburgh,
442 PSE Ltd and the Energy Technologies Partnership who funded his PhD studentship.

443 **Acknowledgments**

444 SBA-15 samples were provided by Dr. Emiliano Fratini and Dr. Piero Baglioni from the
445 University of Florence.

446

447 **References**

- 448 Ahn, H., Lee, C.H., 2004. Effects of capillary condensation on adsorption and thermal desorption
449 dynamics of water in zeolite 13X and layered beds. *Chem. Eng. Sci.* 59, 2727–2743.
450 <https://doi.org/10.1016/j.ces.2004.04.011>
- 451 Ahn, H., Lee, C.H., 2003. Adsorption dynamics of water in layered bed for air-drying TSA process.
452 *AIChE J.* 49, 1601–1609. <https://doi.org/10.1002/aic.690490623>
- 453 Aris, R., 1991. Manners makyth modellers. *Chem. Eng. Sci.* 46, 1535–1544.
454 [https://doi.org/10.1016/0009-2509\(91\)87003-U](https://doi.org/10.1016/0009-2509(91)87003-U)
- 455 Baker, F.S., Sing, K.S.W., 1976. Specificity in the adsorption of nitrogen and water on
456 hydroxylated and dehydroxylated silicas. *J. Colloid Interface Sci.* 55, 605–613.
457 [https://doi.org/10.1016/0021-9797\(76\)90071-0](https://doi.org/10.1016/0021-9797(76)90071-0)
- 458 Brandani, F., Ruthven, D., 2003. Measurement of Adsorption Equilibria by the Zero Length
459 Column (ZLC) Technique Part 2: Binary Systems. *Ind. Eng. Chem. Res.* 42, 1462–1469.
460 <https://doi.org/10.1021/ie020573f>
- 461 Brandani, F., Ruthven, D., Coe, C.G., 2003. Measurement of adsorption equilibrium by the zero
462 length column (ZLC) technique part 1: Single-component systems. *Ind. Eng. Chem. Res.* 42,
463 1451–1461. <https://doi.org/10.1021/ie020572n>
- 464 Brandani, S., 2016. A Simple Graphical Check of Consistency for Zero Length Column
465 Desorption Curves. *Chem. Eng. Technol.* 39, 1194–1198.
466 <https://doi.org/10.1002/ceat.201500634>

467 Brandani, S., 2005. On the chromatographic measurement of equilibrium isotherms using large
468 concentration steps. *Adsorption* 11, 231–235. <https://doi.org/10.1007/s10450-005-5929-0>

469 Brandani, S., 1998. Effects of nonlinear equilibrium on zero length column experiments. *Chem.*
470 *Eng. Sci.* 53, 2791–2798. [https://doi.org/10.1016/S0009-2509\(98\)00075-X](https://doi.org/10.1016/S0009-2509(98)00075-X)

471 Brandani, S., 1996. Analytical solution for ZLC desorption curves with bi-porous adsorbent
472 particles. *Chem. Eng. Sci.* 51, 3283–3288. [https://doi.org/10.1016/0009-2509\(95\)00399-1](https://doi.org/10.1016/0009-2509(95)00399-1)

473 Brandani, S., Jama, M.A., Ruthven, D.M., 2000. ZLC measurements under non-linear conditions.
474 *Chem. Eng. Sci.* 55, 1205–1212. [https://doi.org/10.1016/S0009-2509\(99\)00411-X](https://doi.org/10.1016/S0009-2509(99)00411-X)

475 Brandani, S., Ruthven, D.M., 1996a. Analysis of ZLC desorption curves for gaseous systems.
476 *Adsorption* 2, 133–143. <https://doi.org/10.1007/BF00127043>

477 Brandani, S., Ruthven, D.M., 1996b. Moments Analysis of the Zero Length Column Method. *Ind.*
478 *Eng. Chem. Res.* 35, 315–319. <https://doi.org/10.1021/ie950287m>

479 Canivet, J., Fateeva, A., Guo, Y., Coasne, B., Farrusseng, D., 2014. Water adsorption in MOFs:
480 fundamentals and applications. *Chem. Soc. Rev.* 43, 5594–5617.
481 <https://doi.org/10.1039/C4CS00078A>

482 Centineo, A., Nguyen, H.G.T., Espinal, L., Horn, J.C., Brandani, S., 2019. An experimental and
483 modelling study of water vapour adsorption on SBA-15. *Microporous Mesoporous Mater.*
484 282, 53–72. <https://doi.org/https://doi.org/10.1016/j.micromeso.2019.03.018>

485 Chiang, W.S., Fratini, E., Baglioni, P., Georgi, D., Chen, J.H., Liu, Y., 2016. Methane Adsorption
486 in Model Mesoporous Material, SBA-15, Studied by Small-Angle Neutron Scattering. *J.*

487 Phys. Chem. C 120, 4354–4363. <https://doi.org/10.1021/acs.jpcc.5b10688>

488 Chmelik, C., Kärger, J., 2016. The predictive power of classical transition state theory revealed in
489 diffusion studies with MOF ZIF-8. *Microporous Mesoporous Mater.* 225, 128–132.
490 <https://doi.org/10.1016/j.micromeso.2015.11.051>

491 Cordero, S., Rojas, F., Kornhauser, I., Domínguez, A., Vidales, A.M., López, R., Zgrablich, G.,
492 Riccardo, J.L., 2002. Pore-blocking and pore-assisting factors during capillary condensation
493 and evaporation. *Appl. Surf. Sci.* 196, 224–238. [https://doi.org/10.1016/S0169-](https://doi.org/10.1016/S0169-4332(02)00061-2)
494 [4332\(02\)00061-2](https://doi.org/10.1016/S0169-4332(02)00061-2)

495 Cychosz, K.A., Guillet-Nicolas, R., García-Martínez, J., Thommes, M., 2017. Recent advances in
496 the textural characterization of hierarchically structured nanoporous materials. *Chem. Soc.*
497 *Rev.* 46, 389–414. <https://doi.org/10.1039/c6cs00391e>

498 Duncan, W.L., Moller, K.P., 2002. The effect of a crystal size distribution on ZLC experiments.
499 *Chem. Eng. Sci.* 57, 2641–2652. [https://doi.org/10.1016/S0009-2509\(02\)00161-6](https://doi.org/10.1016/S0009-2509(02)00161-6)

500 Eic, M., Ruthven, D.M., 1988. A new experimental technique for measurement of intracrystalline
501 diffusivity. *Zeolites* 8, 40–45. [https://doi.org/10.1016/S0144-2449\(88\)80028-9](https://doi.org/10.1016/S0144-2449(88)80028-9)

502 Friedrich, D., Mangano, E., Brandani, S., 2015. Automatic estimation of kinetic and isotherm
503 parameters from ZLC experiments. *Chem. Eng. Sci.* 126, 616–624.
504 <https://doi.org/10.1016/j.ces.2014.12.062>

505 Glover, T.G., Wang, Y., Van, M.D. Le, 2008. Diffusion of condensable vapors in single adsorbent
506 particles measured via concentration-swing frequency response. *Langmuir* 24, 13406–13413.

507 <https://doi.org/10.1021/la802222r>

508 Hefti, M., Joss, L., Marx, D., Mazzotti, M., 2015. An Experimental and Modeling Study of the
509 Adsorption Equilibrium and Dynamics of Water Vapor on Activated Carbon. *Ind. Eng.*
510 *Chem. Res.* 54, 12165–12176. <https://doi.org/10.1021/acs.iecr.5b03445>

511 Kärger, J., Ruthven, D.M., Theodorou, D.N., 2012. *Diffusion in Nanoporous Materials*. Copyright
512 © 2012 Wiley- VCH Verlag GmbH & Co. KGaA, Weinheim, Germany.
513 <https://doi.org/10.1002/9783527651276>

514 Klomkliang, N., Do, D.D., Nicholson, D., 2015. Hysteresis loop and scanning curves for argon
515 adsorbed in mesopore arrays composed of two cavities and three necks. *J. Phys. Chem. C*
516 119, 9355–9363. <https://doi.org/10.1021/acs.jpcc.5b01184>

517 Klomkliang, N., Do, D.D., Nicholson, D., 2014. Hysteresis loop and scanning curves of argon
518 adsorption in closed-end wedge pores. *Langmuir* 30, 12879–12887.
519 <https://doi.org/10.1021/la5035992>

520 Lin, T.-F., Little, J.C., Nazaroff, W.W., 1996. Transport and Sorption of Organic Gases in
521 Activated Carbon. *J. Environ. Eng.* 122, 169–175. [https://doi.org/10.1061/\(ASCE\)0733-](https://doi.org/10.1061/(ASCE)0733-9372(1996)122:3(169))
522 [9372\(1996\)122:3\(169\)](https://doi.org/10.1061/(ASCE)0733-9372(1996)122:3(169))

523 Malek, A., Farooq, S., 1996. Effect of velocity variation on equilibrium calculations from
524 multicomponent breakthrough experiments. *Chem. Eng. Sci.* 52, 443–447.
525 [https://doi.org/10.1016/S0009-2509\(96\)00417-4](https://doi.org/10.1016/S0009-2509(96)00417-4)

526 Mangano, E., Brandani, S., Ruthven, D.M., 2013. Analysis and interpretation of zero length

527 column response curves. *Chemie-Ingenieur-Technik* 85, 1714–1718.
528 <https://doi.org/10.1002/cite.201300083>

529 Monson, P.A., 2012. Understanding adsorption/desorption hysteresis for fluids in mesoporous
530 materials using simple molecular models and classical density functional theory.
531 *Microporous Mesoporous Mater.* 160, 47–66.
532 <https://doi.org/10.1016/j.micromeso.2012.04.043>

533 Morishige, K., 2017. Dependent Domain Model of Cylindrical Pores. *J. Phys. Chem. C* 121, 5099–
534 5107. <https://doi.org/10.1021/acs.jpcc.6b12566>

535 Naono, H., Fujiwara, R., Yagi, M., 1980. Determination of physisorbed and chemisorbed waters
536 on silica gel and porous silica glass by means of desorption isotherms of water vapor. *J.*
537 *Colloid Interface Sci.* 76, 74–82. [https://doi.org/10.1016/0021-9797\(80\)90272-6](https://doi.org/10.1016/0021-9797(80)90272-6)

538 Nguyen, V.T., Horikawa, T., Do, D.D., Nicholson, D., 2014. Water as a potential molecular probe
539 for functional groups on carbon surfaces. *Carbon N. Y.* 67, 72–78.
540 <https://doi.org/10.1016/j.carbon.2013.09.057>

541 Qiu, L., Zhang, M., Tang, J., Adhikari, B., Cao, P., 2019. Innovative technologies for producing
542 and preserving intermediate moisture foods: A review. *Food Res. Int.* 116, 90–102.
543 <https://doi.org/10.1016/J.FOODRES.2018.12.055>

544 Rajniak, P., Yang, R.T., 1993. A Simple Model and Experiments for Adsorption- Desorption
545 Hysteresis : Water Vapor on Silica Gel 39.

546 Ruthven, D.M., 1984. *Principles of Adsorption and Adsorption Processes*, Wiley-Interscience

547 publication. Wiley, New York.

548 Ruzhu Wang; Liwei Wang; Jingyi Wu, 2014. Adsorption Refrigeration Technology: Theory and
549 Application. Copyright © 2014 John Wiley & Sons, Singapore Pte. Ltd., Singapore.
550 <https://doi.org/10.1002/9781118197448>

551 Sarkisov, L., Centineo, A., Brandani, S., 2017. Molecular simulation and experiments of water
552 adsorption in a high surface area activated carbon: Hysteresis, scanning curves and spatial
553 organization of water clusters. Carbon N. Y. 118, 127–138.
554 <https://doi.org/10.1016/j.carbon.2017.03.044>

555 Thommes, M., Cychosz, K.A., Neimark, A. V, 2012. Chapter 4 - Advanced Physical Adsorption
556 Characterization of Nanoporous Carbons, in: Tascón, J.M.D. (Ed.), Novel Carbon
557 Adsorbents. Elsevier, Oxford, pp. 107–145. [https://doi.org/https://doi.org/10.1016/B978-0-](https://doi.org/https://doi.org/10.1016/B978-0-08-097744-7.00004-1)
558 [08-097744-7.00004-1](https://doi.org/https://doi.org/10.1016/B978-0-08-097744-7.00004-1)

559 Thommes, M., Kaneko, K., Neimark, A. V., Olivier, J.P., Rodriguez-Reinoso, F., Rouquerol, J.,
560 Sing, K.S.W., 2015. Physisorption of gases, with special reference to the evaluation of surface
561 area and pore size distribution (IUPAC Technical Report). Pure Appl. Chem. 87, 1051–1069.
562 <https://doi.org/10.1515/pac-2014-1117>

563 Thommes, M., Morell, J., Cychosz, K.A., Fröba, M., 2013. Combining Nitrogen, Argon, and
564 Water Adsorption for Advanced Characterization of Ordered Mesoporous Carbons (CMKs)
565 and Periodic Mesoporous Organosilicas (PMOs). Langmuir 29, 14893–14902.
566 <https://doi.org/10.1021/la402832b>

567 Thommes, M., Morlay, C., Ahmad, R., Joly, J.P., 2011. Assessing surface chemistry and pore

568 structure of active carbons by a combination of physisorption (H₂O, Ar, N₂, CO₂), XPS and
569 TPD-MS. *Adsorption* 17, 653–661. <https://doi.org/10.1007/s10450-011-9360-4>

570 Tompsett, G.A., Krogh, L., Griffin, D.W., Conner, W.C., 2005. Hysteresis and scanning behavior
571 of mesoporous molecular sieves. *Langmuir* 21, 8214–8225.
572 <https://doi.org/10.1021/la050068y>

573 Velasco, L.F., Guillet-Nicolas, R., Dobos, G., Thommes, M., Lodewyckx, P., 2016. Towards a
574 better understanding of water adsorption hysteresis in activated carbons by scanning
575 isotherms. *Carbon N. Y.* 96, 753–758. <https://doi.org/10.1016/j.carbon.2015.10.017>

576 Wang, H., Brandani, S., Lin, G., Hu, X., 2011. Flowrate correction for the determination of
577 isotherms and Darken thermodynamic factors from Zero Length Column (ZLC) experiments.
578 *Adsorption* 17, 687–694. <https://doi.org/10.1007/s10450-011-9364-0>

579 Waterman, K.C., Macdonald, B.C., 2010. Package Selection for Moisture Protection for Solid,
580 Oral Drug Products. *J. Pharm. Sci.* 99, 4437–4452. <https://doi.org/10.1002/JPS.22161>

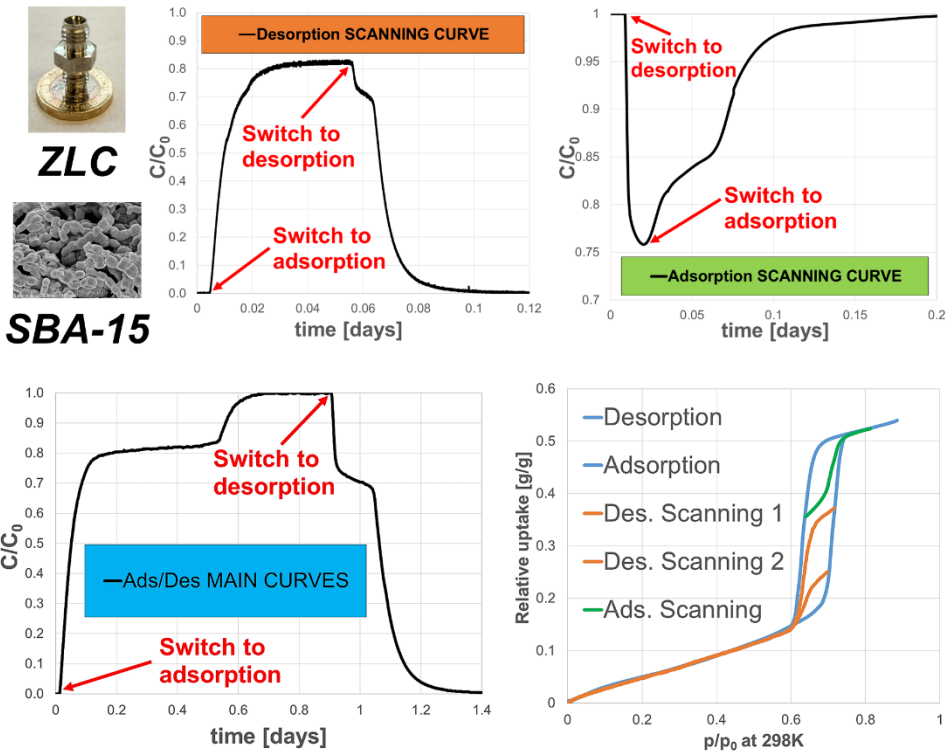
581 Young, J.F., 2007. Humidity control in the laboratory using salt solutions—a review. *J. Appl.*
582 *Chem.* 17, 241–245. <https://doi.org/doi:10.1002/jctb.5010170901>

583 Zeng, Y., Tan, S.J., Do, D.D., Nicholson, D., 2016. Hysteresis and scanning curves in linear arrays
584 of mesopores with two cavities and three necks. Classification of the scanning curves.
585 *Colloids Surfaces A Physicochem. Eng. Asp.* 496, 52–62.
586 <https://doi.org/10.1016/j.colsurfa.2015.08.023>

587

588

589 Abstract Graphic



590

591

592

593

594

595

596

597

598

599

600

601

602 **List of figures**

603 **Fig. 1.** (A) Adsorption-Desorption equilibrium isotherm and ZLC response curves simulated under
604 equilibrium control conditions. Linear isotherm. (B) Adsorption-Desorption equilibrium isotherm
605 and ZLC response curves simulated under equilibrium control conditions. Type I isotherm. (C)
606 Adsorption-Desorption equilibrium isotherm and ZLC response curves simulated under
607 equilibrium control conditions. Type IV isotherm.

608

609 **Fig. 2.** Schematic flowsheet and components of the experimental ZLC system. GC carrier gas
610 cylinder; DC drying column; BV ball valve; NV needle valve; TC water bath temperature
611 controller; MFC mass flow controllers; B water bath; SV solenoid switching valve; V vent; O ZLC
612 oven; ZLC zero length column; DPT differential pressure transducer; HP humidity probe; MS
613 mass spectrometer.

614

615 **Fig. 3.** SEM image of SBA-15 sample used in this study.

616

617 **Fig. 4.** Experimental *Ft*-plot for the evaluation of the control regime. Sample mass 1.2 mg. Initial
618 relative humidity = 86 %, at 298K and atmospheric pressure.

619

620 **Fig. 5.** Desorption isotherm calculated by using the two lowest flowrates shown in Fig. 4. Sample
621 mass 1.2 mg. Initial relative humidity = 86 % at 298K and atmospheric pressure.

622

623 **Fig. 6.** Experimental response curves for the blank column and packed column. Sample mass 3.7
624 mg. Initial relative humidity = 86 % at 298K and atmospheric pressure.

625

626 **Fig. 7.** Adsorption and desorption isotherms measured using two different sample masses. Initial
627 relative humidity = 86 % and atmospheric pressure.

628

629 **Fig. 8.** Comparison between the isotherms measured with the ZLC system and gravimetric system.
630 ZLC sample mass 3.7 mg. Gravimetric sample mass 7 mg. Initial relative humidity = 86 % and
631 atmospheric pressure. Experimental signals are shown in Fig. 9.

632

633 **Fig. 9.** (A) Experimental adsorption-desorption normalized response curves measured under
634 equilibrium control conditions on the ZLC. (B) Adsorbed phase concentration vs time obtained
635 from ZLC mass balance. Sample mass 3.7 mg. Highest relative humidity = 86 % at 298K and
636 atmospheric pressure. (C) Experimental uptake curves obtained from the measurement of the
637 equilibrium adsorption-desorption isotherm on the gravimetric system. Sample mass 7 mg.

638

639 **Fig. 10.** Experimental normalized response curves measured under equilibrium control conditions
640 on the ZLC at 298K and atmospheric pressure. Sample mass 3.7 mg. (A) Measurement of the main
641 adsorption branch. Final relative humidity = 86 %. (B) Measurement of the main desorption
642 branch. Initial relative humidity = 86 %.

643

644 **Fig. 11.** Experimental adsorption-desorption isotherm calculated from the ZLC response curves
645 shown in Fig. 10. Sample mass 3.7 mg. Highest relative humidity = 86 % at 298K and atmospheric
646 pressure.

647

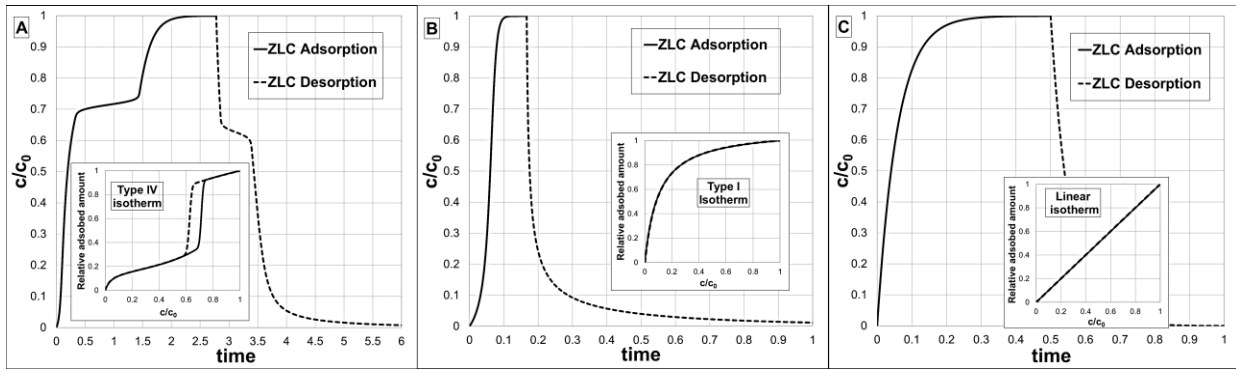
648 **Fig. 12.** Experimental adsorption-desorption normalized response curve measured under
649 equilibrium control conditions at 298K and atmospheric pressure for sample mass 3.7 mg. (A)
650 Measurement of the desorption scanning curve, $t_{\text{switch}} = 12110$ s. Initial relative humidity = 71.5
651 %. (B) Measurement of the adsorption scanning curve, $t_{\text{switch}} = 1710$ s. Initial relative humidity =
652 64 %.

653

654 **Fig. 13.** (A) Desorption scanning curves measured on the ZLC system and gravimetric system.
655 Initial relative humidity = 72.2 %, 71.5 % and, 69.7 %. ZLC sample mass 3.7 mg. Gravimetric
656 sample mass 7 mg. (B) Adsorption scanning curves measured on the ZLC system and gravimetric
657 system. Initial relative humidity = 64 % and, 64.8 %. ZLC sample mass 3.7 mg at 298K and
658 atmospheric pressure. Gravimetric sample mass 7 mg.

659

660
661



662

663

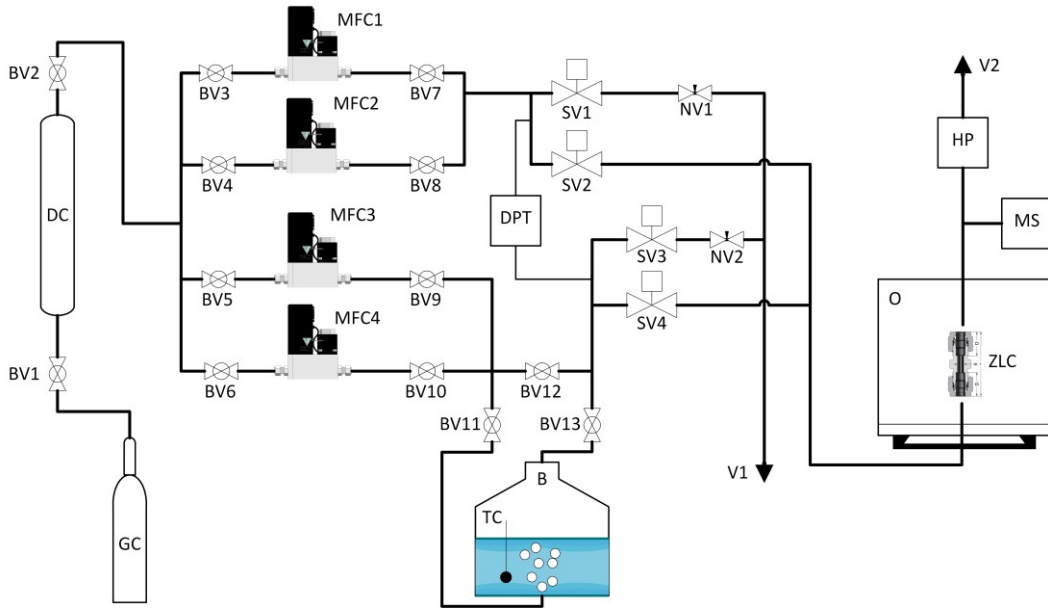
664

665

666 **Fig. 1.** (A) Adsorption-Desorption equilibrium isotherm and ZLC response curves simulated under
667 equilibrium control conditions. Linear isotherm. (B) Adsorption-Desorption equilibrium isotherm
668 and ZLC response curves simulated under equilibrium control conditions. Type I isotherm. (C)
669 Adsorption-Desorption equilibrium isotherm and ZLC response curves simulated under
670 equilibrium control conditions. Type IV isotherm.

671

672



673

674

675

676 **Fig. 2.** Schematic flowsheet and components of the experimental ZLC system. GC carrier gas
677 cylinder; DC drying column; BV ball valve; NV needle valve; TC water bath temperature
678 controller; MFC mass flow controllers; B water bath; SV solenoid switching valve; V vent; O ZLC
679 oven; ZLC zero length column; DPT differential pressure transducer; HP humidity probe; MS
680 mass spectrometer.

681

682



683

684

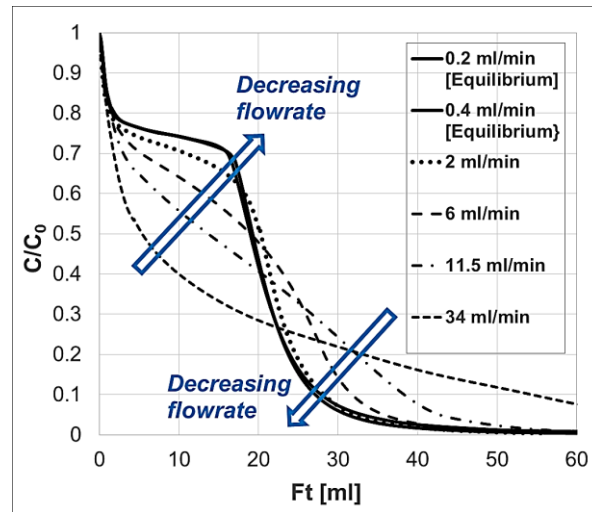
685

686

687 **Fig. 3.** SEM image of SBA-15 sample used in this study.

688

689



690

691

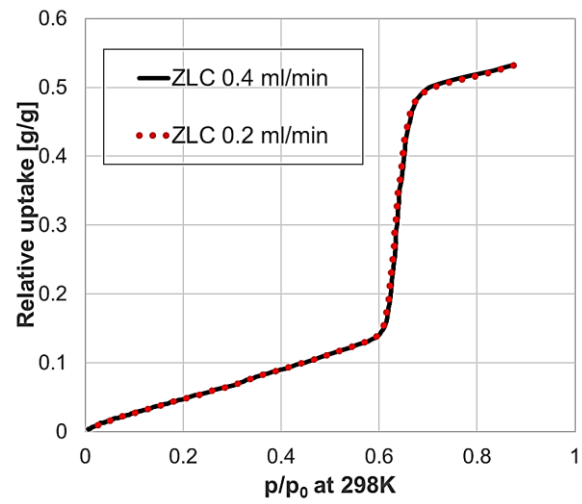
692

693

694 **Fig. 4.** Experimental Ft -plot for the evaluation of the control regime. Sample mass 1.2 mg. Initial
695 relative humidity = 86 %, at 298K and atmospheric pressure.

696

697



698

699

700

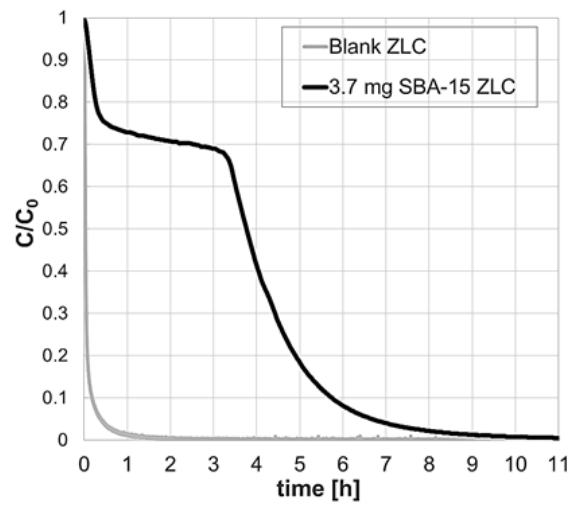
701

702 **Fig. 5.** Desorption isotherm calculated by using the two lowest flowrates shown in Fig. 4. Sample

703 mass 1.2 mg. Initial relative humidity = 86 % at 298K and atmospheric pressure.

704

705



706

707

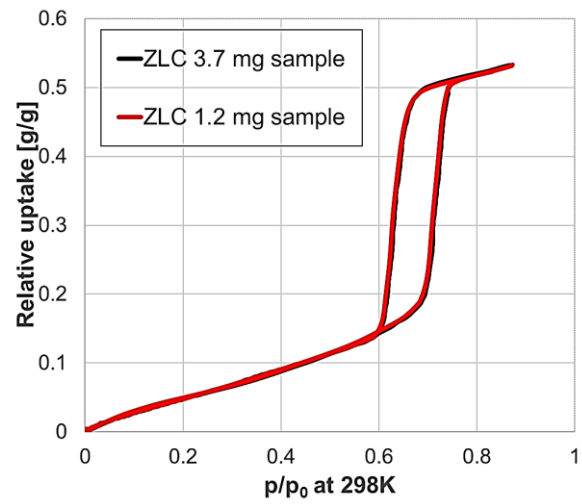
708

709 **Fig. 6.** Experimental response curves for the blank column and packed column. Sample mass 3.7
710 mg. Initial relative humidity = 86 % at 298K and atmospheric pressure.

711

712

713



714

715

716

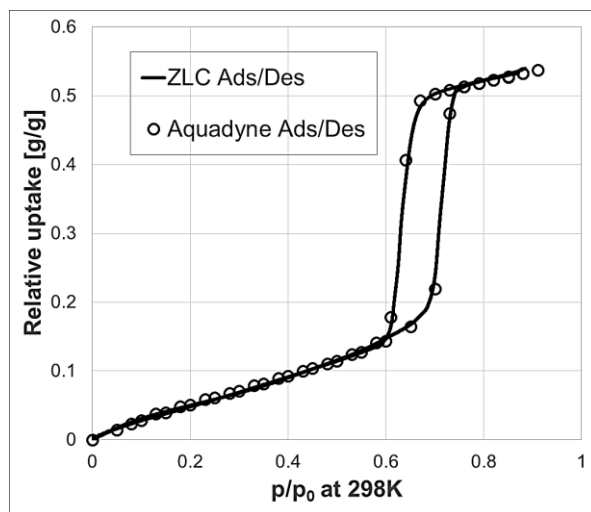
717

718 **Fig. 7.** Adsorption and desorption isotherms measured using two different sample masses. Initial

719 relative humidity = 86 % and atmospheric pressure.

720

721



722

723

724

725

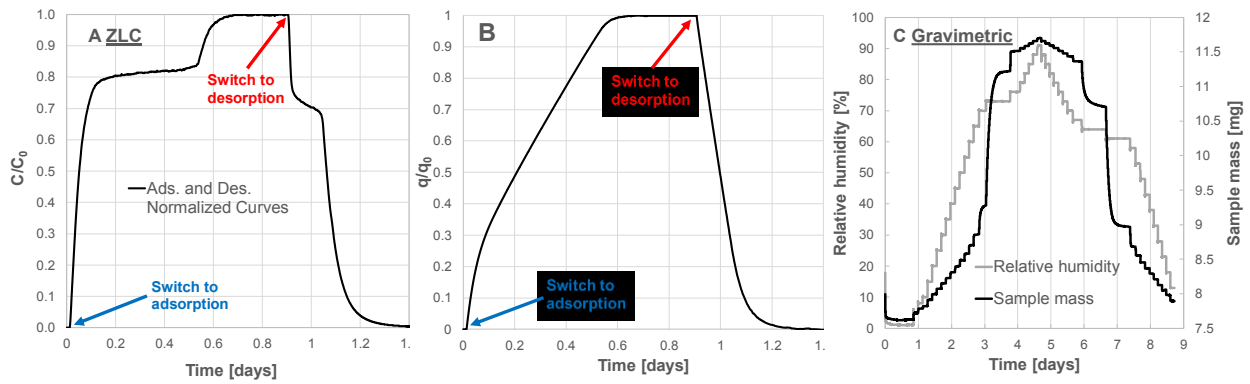
726 **Fig. 8.** Comparison between the isotherms measured with the ZLC system and gravimetric system.

727 ZLC sample mass 3.7 mg. Gravimetric sample mass 7 mg. Initial relative humidity = 86 % and

728 atmospheric pressure. Experimental signals are shown in Fig. 9.

729

730



731

732

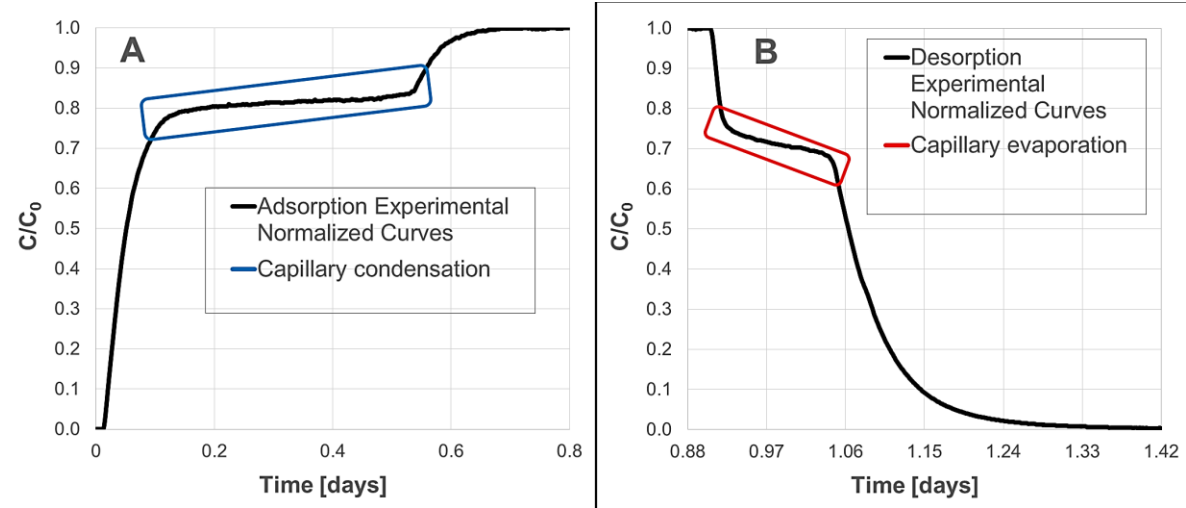
733

734

735 **Fig. 9.** (A) Experimental adsorption-desorption normalized response curves measured under
736 equilibrium control conditions on the ZLC. (B) Adsorbed phase concentration vs time obtained
737 from ZLC mass balance. Sample mass 3.7 mg. Highest relative humidity = 86 % at 298K and
738 atmospheric pressure. (C) Experimental uptake curves obtained from the measurement of the
739 equilibrium adsorption-desorption isotherm on the gravimetric system. Sample mass 7 mg.

740

741



742

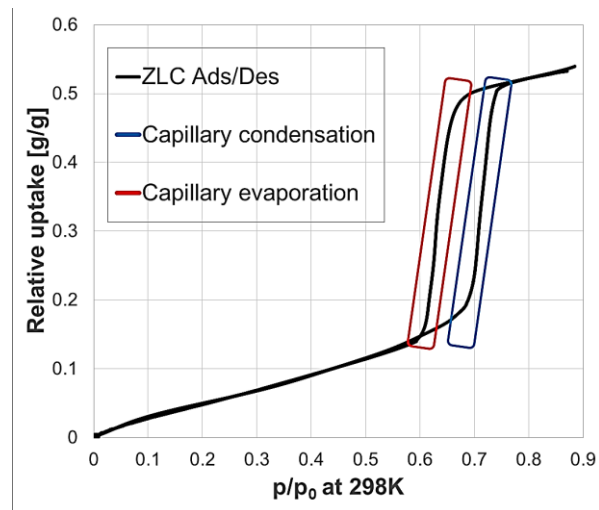
743

744

745 **Fig. 10.** Experimental normalized response curves measured under equilibrium control conditions
746 on the ZLC at 298K and atmospheric pressure. Sample mass 3.7 mg. (A) Measurement of the main
747 adsorption branch. Final relative humidity = 86 %. (B) Measurement of the main desorption
748 branch. Initial relative humidity = 86 %.

749

750



751

752

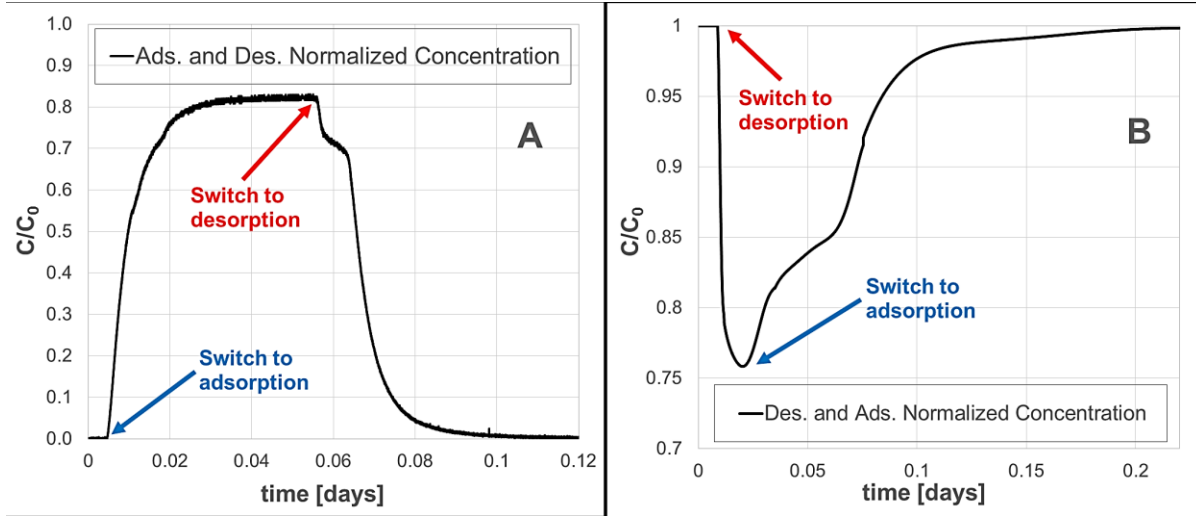
753

754

755 **Fig. 11.** Experimental adsorption-desorption isotherm calculated from the ZLC response curves
756 shown in Fig. 10. Sample mass 3.7 mg. Highest relative humidity = 86 % at 298K and atmospheric
757 pressure.

758

759



760

761

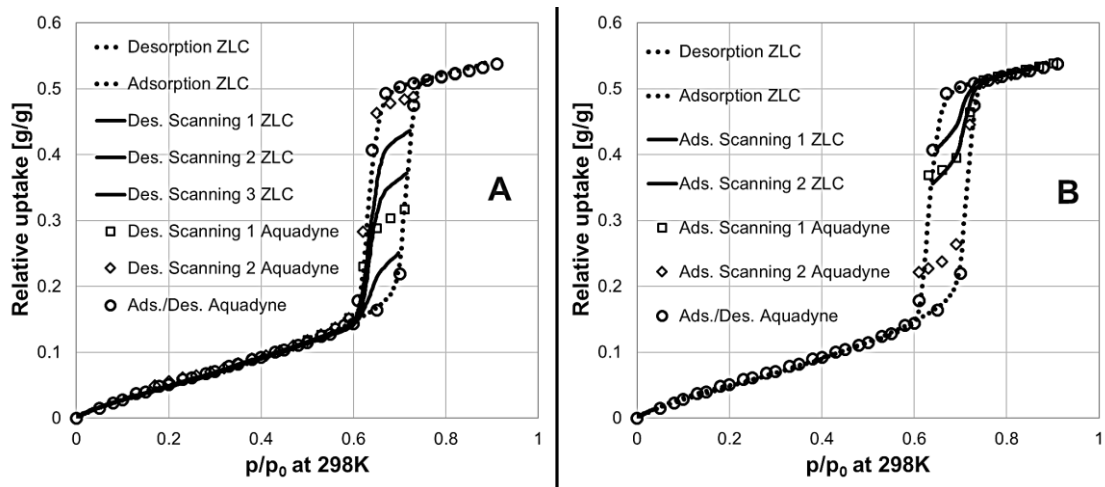
762

763

764 **Fig. 12.** Experimental adsorption-desorption normalized response curve measured under
765 equilibrium control conditions at 298K and atmospheric pressure for sample mass 3.7 mg. (A)
766 Measurement of the desorption scanning curve, $t_{\text{switch}} = 12110$ s. Initial relative humidity = 71.5
767 %. (B) Measurement of the adsorption scanning curve, $t_{\text{switch}} = 1710$ s. Initial relative humidity =
768 64 %.

769

770



771

772

773

774

775 **Fig. 13.** (A) Desorption scanning curves measured on the ZLC system and gravimetric system.

776 Initial relative humidity = 72.2 %, 71.5 % and, 69.7 %. ZLC sample mass 3.7 mg. Gravimetric

777 sample mass 7 mg. (B) Adsorption scanning curves measured on the ZLC system and gravimetric

778 system. Initial relative humidity = 64 % and, 64.8 %. ZLC sample mass 3.7 mg at 298K and

779 atmospheric pressure. Gravimetric sample mass 7 mg.

780

781